

## Supplemental Information

### S.1. Methods

All of the calculations reported herein were carried out using periodic, plane-wave density functional theory (DFT) calculations using the Vienna ab initio Simulation Program (VASP) [S1]. The wave functions were constructed from a series of plane-wave basis functions expanded out to an energy cutoff of 396 eV using the Perdew-Wang form of the generalized-gradient approximation (PW91) [S2]. Electron-ion interactions were described through the use of Vanderbilt ultrasoft pseudopotentials [S3]. The surface Brillouin zone was sampled with a 3x2x1 Monkhorst-Pack k-point grid. The electronic energies were converged to within  $1 \times 10^{-6}$  eV.

Experimental results show that both esterification and condensation rates increase with increasing particle size.[S4] Metal particles  $> 5$  nm are predominantly comprised ( $> 90\%$ ) of coordinatively-saturated metal terrace sites suggesting that they are active sites. The simulations were therefore predominantly carried out over Cu(111) surface to mimic the terraces of the large supported Cu clusters. The Cu(111) surface was modeled using a four-layer slab comprised of 18 Cu atoms in each layer in a (3x6) surface unit cell. A vacuum region of 10 Å was included between metal slabs to prevent any interactions between the slabs. The bottom two layers of the Cu substrate were held fixed throughout the structural optimizations at their bulk positions with Cu-Cu distance of 2.55 Å. All structures were optimized until the maximum forces on all of the atoms were less than  $0.05 \text{ eV \AA}^{-1}$ . The influence of edge and corner sites on the activation of C-H and O-H bonds of propanol were also examined by carrying out calculations on a Cu110 surface and on a 201 atom cuboctahedral Cu cluster ( $\text{Cu}_{201}$ ) where all of the Cu atoms were allowed to relax.

The adsorption energies for all of the reactant and product molecules were calculated as:

$$\Delta E_{\text{ads}} = E_{\text{surf+ads}} - E_{\text{surf}} - E_{\text{ads}} \quad (\text{S1})$$

where  $E_{\text{surf+ads}}$ ,  $E_{\text{surf}}$ , and  $E_{\text{ads}}$  are the energies of the surface-adsorbate complex, the bare metal surface, and the adsorbate in vacuum, respectively. For reactions, the activation barriers and reaction energies were calculated as:



$$\Delta E_{\text{ACT}} = E_{\text{TS}^*} + \delta E_{\text{surf}} - E_{A^*} - E_{B^*} \quad (\text{S3})$$

$$\Delta E_{\text{RXN}} = E_{C^*} + E_{D^*} - E_{A^*} - E_{B^*} \quad (\text{S4})$$

where  $E_{i^*}$  and  $E_{TS^*}$  refer to the energies of adsorbed intermediate  $i$  ( $A^*$ ,  $B^*$ ,  $C^*$  or  $D^*$ ) and the transition state ( $TS^*$ ), respectively.  $\delta E_{surf}$  refers to the change in energy required to bring the “infinitely” separated species on the surface together into the reactant state where they sit adjacent to one another thus accounting for any attractive or repulsive interactions.

Activation barriers were determined using a two-step transition state search scheme. In the first step, the nudged elastic band (NEB) method [S5-S7] was used to determine the minimum energy reaction path and establish a reliable first guess of the transition state. The highest energy image along the minimum energy path was used as an initial guess of the transition state structure and used in the Dimer method [S8-S9] to isolate the transition state structure and minimize the forces on all of the atoms in the structure to below  $0.03 \text{ eV \AA}^{-1}$ . The intrinsic activation barriers for the elementary steps reported herein all refer to the direct energy difference between the transition state and the bound reactant(s) state along the elementary step reaction coordinate ( $E_{TS^*} - E_{A^*} - E_{B^*}$  in Eq. 3). In order to compare with experimental results, we also calculate apparent activation energies where the transition state energies are referenced to the most abundant species present on the surface under reaction conditions rather than from the elementary step reactant state. Experimental results suggest that the reactions are carried out at higher surface coverages under working conditions. . We therefore use adsorbed propoxide and the gas phase alkanal as the zero energy reference state to calculate apparent barriers for most of the systems discussed herein.

The enthalpy, entropy and free energies of activation were calculated for the rate controlling esterification and condensation steps. The Gibbs free energy of activation for the reaction between two surface intermediates can be calculated by:

$$G^\ddagger = -RT \ln \left( \frac{q_{vib}^{TS}}{q_{vib}^R} \right) \quad (S5)$$

where,  $R$  is the ideal gas constant,  $T$  is the temperature,  $q_{vib}^{TS}$  and  $q_{vib}^R$  are vibrational partition functions of the transition state and the reactant state, respectively. The vibrational frequencies and the vibrational corrections to the electronic and internal energies were calculated within VASP on the optimized structure using the quasi-harmonic approximation. For frequency calculations, the electronic energies were converged to within  $10^{-8} \text{ eV}$  and a step size of  $0.015 \text{ \AA}$  was used. The reaction enthalpies and activation enthalpies were estimated by applying translational and rotational corrections to the internal energy. The vibrational frequencies were subsequently used to calculate the vibration partition functions of the

reactant, transition and product states. The results were used to calculate the free energies of activation. The activation entropies were back-calculated from the free energies and enthalpies

The charges for reactant, product and transition states were calculated by using quasi-atomic minimal basis set orbitals (QUAMBO) [S10] which recreate the electron density determined using VASP.

### S.2 Activation of propanol on coordinatively unsaturated Cu sites.

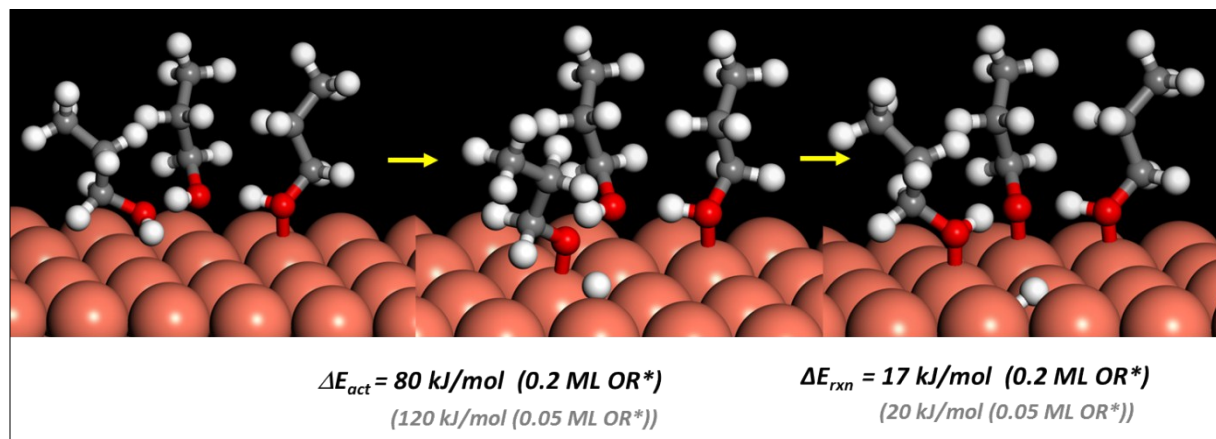


**Figure S1.** Influence of higher coverage on the dissociation of propanal over Cu(111). Higher coverages of propanal decrease the barrier by 40 kJ/mol to activate propanol by allowing for proton-coupled electron shuttling paths.

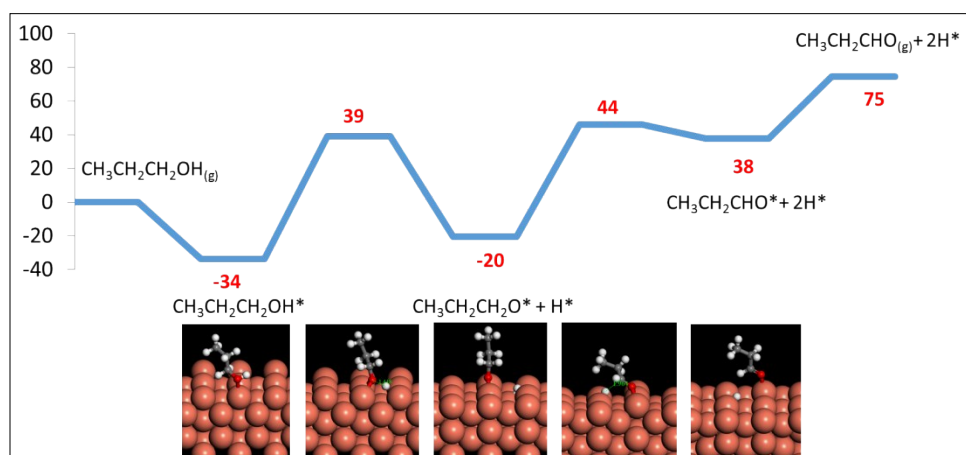


**Figure S2.** DFT-calculated activation barriers and reaction energies for the adsorption and dissociation of propanol to propoxide and  $\text{H}^*$  and the subsequent reaction of propoxide to propanal and hydrogen over the Cu(110) surface.

### S.3 Charge transfer in adsorbed hydroxides and alkoxides on different transition metals.

The charge transfer to the O of HO upon its adsorption to different 3d, 4d and 5d transition metals ranges from  $-0.77 e^-$  on the more oxophillic metals (Pd, Rh and Ru) which bind O strongly to  $-1.04 e^-$

1.07 e<sup>-</sup> on the group 11 metals (Cu, Ag, Au) which bind O\* weakly as shown in Table S1 of the supplemental. Similarly, charge transfer from the metal to the O-atom in the adsorbed alkoxide (RO\*) results in a charge on the oxygen that ranges from -0.54 on Rh and Ru to -0.83 e<sup>-</sup> on Cu, Ag, and Au. The results indicate that both RO\* and HO\* species on group 11 metal (Cu, Ag and Au) surfaces act as bases as they extract electron density from the metal and become negatively charged (Table S1). The charge transferred to the RO\* and HO\* species from other metals is significantly less than that from group 11 metals, likely due to the high electron density in the nearly-filled d-bands of these coinage metals (Cu: 3d<sup>10</sup>; Ag: 4d<sup>10</sup>; Au: 5d<sup>10</sup>).

**Table S1.** Summary of the charge accumulated on O atom for adsorbed HO\* and CH<sub>3</sub>O\* groups bound to different transition metal (111) surfaces.

<i>Species</i>	<i>Metal</i>	<i>Charge on O after ads.</i>	<i>Species</i>	<i>Metal</i>	<i>Charge on O after ads.</i>
<b>HO*</b> -0.44 <sup>a</sup>	<b>Cu</b>	-1.05	<b>CH<sub>3</sub>O*</b> -0.33 <sup>a</sup>	Cu	-0.83
	<b>Au</b>	-1.04		Au	-0.77
	<b>Ag</b>	-1.07		Ag	-0.81
	<b>Pd</b>	-0.79		Pd	-0.56
	<b>Ru</b>	-0.77		Ru	-0.54
	<b>Rh</b>	-0.77		Rh	-0.55

<sup>a</sup> The number in the bracket is the charge on the O of OH/OR before

#### S.4 Discussion of Aldol Condensation Paths

In all three paths, we assume, based on the results presented in section 3.2 in the paper, that propanal and hydrogen are equilibrated with propanol. For simplicity, all of the paths in Figure S3 are therefore referenced to the same adsorbed propanal and propoxide initial state defined as E=0.

The results in Figure S3a show that the reaction does not proceed through the dehydrogenation of the adsorbed propanal to an acyl intermediate as it would require an apparent barrier of 160 kJ mol<sup>-1</sup> taken with respect to the adsorbed propoxide and propanal. The two paths which proceed via the coupling of propanal and propoxide to form the β-hydroxide alkanal are significantly lower in energy and more viable than the acyl path. The energy diagrams in Figure S3 indicate that the rates for the paths involving the coupling of propoxide and propanal are ultimately dictated by the barrier for enolate formation which involves the abstraction the weakly acidic H of C<sub>2α</sub>-H of the adsorbed alkanal. The barrier for enolate formation was calculated to be 70 kJ mol<sup>-1</sup> taken with respect to the adsorbed propoxide and propanal which are the most abundant species on the surface. The β-hydroxide alkanal that results from C-C bond formation subsequently reacts by: 1) H\* addition to form the aldol which reacts to form 2-methyl-

pentanal and 2-methyl-3-pentanone products or 2) hydride transfer to an adsorbed propanal that goes on to form 3-pentanone.

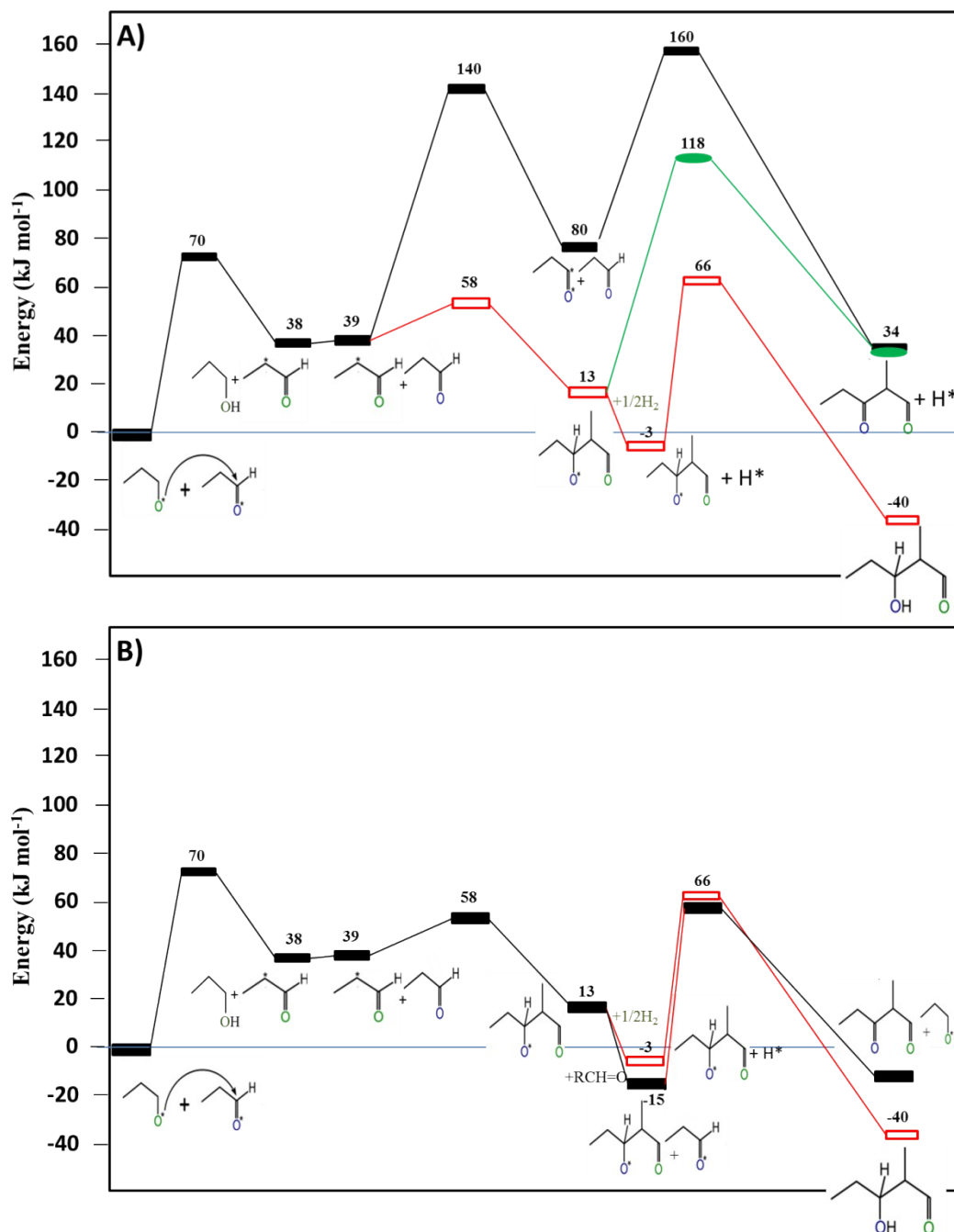


**Figure S3.** DFT-calculated pathways for the aldol condensation reactions of propanol-propanal on Cu(111). A) The upper path (shown with black filled rectangular symbols) proceeds via the initial activation of the propyl to form an acyl

intermediate which is high in energy. The middle path (shown with lighter filled oval symbols) proceeds via the coupling of the enolate and propanal followed by C<sub>1</sub>-H activation by the Cu, whereas the lowest energy path (unfilled rectangular symbols) proceeds by the coupling of the enolate and propanal to form the β-alkoxide alkanal which subsequently hydrogenates to form the aldol. B) The two lowest energy paths shown here proceed via the coupling of the enolate and propanal to form the β-alkoxide alkanal which can: i) hydrogenate (shown with unfilled rectangular symbols) to form the aldol or ii) dehydrogenate via hydride transfer an adsorbed propanal to form 2-formyl-3-pentanone (shown with filled black rectangular symbols).

The rate for both propoxide and propanal coupling reactions are controlled by the initial activation of the weakly acidic C<sub>2α</sub>-H bond on the alkanal by a basic propoxide surface intermediate and can be written as:

$$r_{cond} = k_{cond}[\text{propanal}^*][\text{propoxide}^*]$$

$$= k_{cond}K_{PAL}^2K_{HYD1}K_{H2}^{1/2}P_{PAL}^2P_{H2}^{1/2}/[1 + K_{PAL}P_{PAL} + K_{PAL}K_{HYD1}K_{H2}^{1/2}P_{PAL}P_{H2}^{1/2}]^2 \quad (\text{S6})$$

where  $k_{cond}$  refers to the intrinsic rate constant for deprotonation of the weakly acidic C<sub>2α</sub>-H bond;  $K_{PAL}$ ,  $K_{HYD1}$  and  $K_{H2}$  are the equilibrium constants for the adsorption of propanal, the hydrogenation of propanal to the surface propoxide over Cu and the dissociative adsorption of hydrogen, respectively, and  $P_{AL}$  and  $P_{H2}$  refer to the partial pressure of propanal and hydrogen, respectively. The apparent activation barrier for this path calculated with respect to the adsorbed propanal and propoxide is simply the 70 kJ mol<sup>-1</sup> barrier for the initial C<sub>2α</sub>-H activation by the propoxide to form the enolate (Fig. S3a). The theoretical results suggest that propanal and propoxide may be abundant surface intermediates. Experimentally-measured rates of reaction as a function of the pressures of propanal and hydrogen indicate that while both propanal and propoxide exist on the surface, the propanal is the most abundant surface intermediate [S4].

## S.5. Esterification Pathways

The elementary steps and corresponding activation and reaction energies for the 3 esterification paths presented in scheme 5 in the manuscript were used to establish the operative rate equations and determine the lowest energy paths shown in Figure S4 and the kinetics for esterification. For simplicity, all three paths presented in Figure S4 are referenced to adsorbed propanal and propoxide as these species rapidly equilibrate as was discussed in section 3.2 in the manuscript.

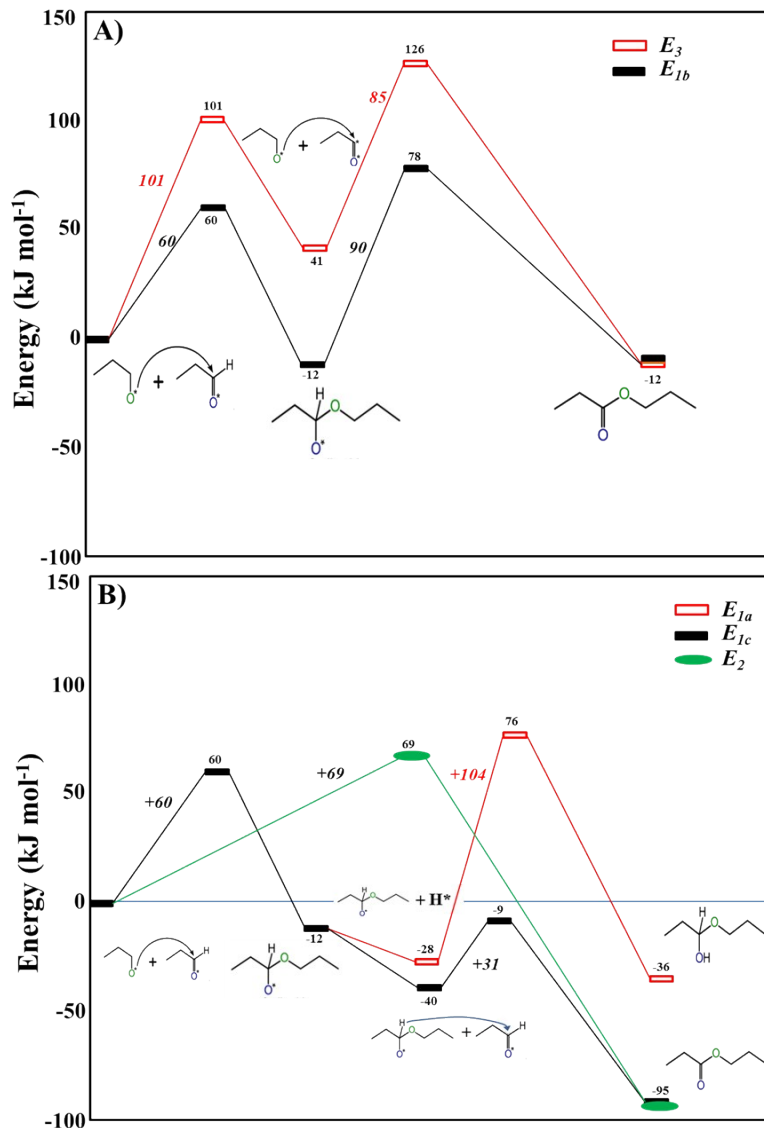


**Figure S4.** DFT-calculated reaction paths for the esterification of propanol-propanol on Cu(111). (A). The  $E_3$  path (light unfilled symbols) which is highest energy proceeds via the C-H activation of propanal to form a surface acyl intermediate that subsequently couples with a bound propanal to form propyl propionate. The  $E_{1b}$  path (filled black symbols) which is lower in energy than the  $E_3$  path, proceeds by the coupling of the alkoxide and the alkanal to form the 1-propoxy-1-propoxide hemiacetalate intermediate that subsequently undergoes C<sub>1</sub>-H activation over Cu to form propyl propionate. The lowest energy paths ( $E_{1a}$ ,  $E_{1c}$  and  $E_2$ ) are shown in (B). In the  $E_{1c}$  path (light unfilled rectangular symbols) the reaction proceeds via the coupling of the alkoxide and the alkanal followed by a hydrogen addition to the hemiacetalate to form the hemiacetal product. The  $E_{1c}$  and  $E_3$  paths are somewhat lower in energy than the  $E_3$  path. The  $E_{1c}$  path which is shown with filled black rectangular symbols proceed via the coupling of propoxide and propanal to form the hemiacetalate intermediate that subsequently reacts with a vicinal propanal to eliminate H to form the propyl propionate. The  $E_3$  path proceeds via a concerted coupling of the surface propyl and propanal intermediates together with the C<sub>1</sub>-H activation by Cu.

The three paths presented in scheme 5 (and in Figure S4) proceed via reactions involving surface bound propoxide and propanal intermediates. These paths are similar in nature to those reported previously for methanol [S11-S12] and ethanol [S13] esterification over Au. All three of the  $E_1$  paths as well as the  $E_2$  path proceed via coupling of the surface propoxide and propanal to form the hemiacetalate or hemiacetal directly, and as such, show similarities in their mechanisms and rate expressions. These paths differ in the subsequent reactions that lead to different products. The potential energy surfaces reported in Figures S4 indicate that the rates for path  $E_{1a}$ ,  $E_{1b}$ ,  $E_{1c}$  paths are controlled by C<sub>1</sub>-H activation of the 1-propoxy-1-propoxide over Cu, H-addition to the 1-propoxy-1-propoxide, and coupling of surface propoxide and propanal, respectively. The rate controlling step in the  $E_2$  path involves the simultaneous coupling of the adsorbed propoxide and propanal together with the direct activation of the C<sub>1</sub>-H bond by Cu. Despite the differences in the rate controlling step, the rate equations for the  $E_1$  and  $E_2$  paths are all very similar and can be written as:

$$\begin{aligned} r_{E1a} &= k_{E1a}[1\text{-propoxy-propoxide}^*] = k_{E1a} K_{C-O}[\text{propanal}^*][\text{propoxide}^*] \\ &= k_{E1a} K_{C-O} K_{PAL}^2 K_{HYD} K_{H_2}^{1/2} P_{PAL}^2 P_{H_2}^{1/2} / [1 + K_{PAL} P_{PAL} + K_{PAL} K_{HYD1} K_{H_2}^{1/2} P_{PAL} P_{H_2}^{1/2}] \quad (S7) \end{aligned}$$

$$\begin{aligned} r_{E1b} &= k_{E1b}[1\text{-propoxy-propoxide}^*][H^*] = k_{E1b} K_{HYD}[\text{propanal}^*][\text{propoxide}^*][H^*] \\ &= k_{E1b} K_{Hadd} K_{PAL}^2 K_{HYD} K_{H_2} P_{PAL}^2 P_{H_2} / [1 + K_{PAL} P_{PAL} + K_{PAL} K_{HYD1} K_{H_2}^{1/2} P_{PAL} P_{H_2}^{1/2}]^2 \quad (S8) \end{aligned}$$

$$\begin{aligned} r_{E1c} &= k_{E1c}[\text{propanal}^*][\text{propoxide}^*] \\ &= k_{E1c} K_{PAL}^2 K_{HYD} K_{H_2}^{1/2} P_{PAL}^2 P_{H_2}^{1/2} / [1 + K_{PAL} P_{PAL} + K_{PAL} K_{HYD1} K_{H_2}^{1/2} P_{PAL} P_{H_2}^{1/2}]^2 \quad (S9) \end{aligned}$$

$$\begin{aligned} r_{E2} &= k_{E2}[\text{propanal}^*][\text{propoxide}^*] \\ &= k_{E2} K_{PAL}^2 K_{HYD} K_{H_2}^{1/2} P_{PAL}^2 P_{H_2}^{1/2} / [1 + K_{PAL} P_{PAL} + K_{PAL} K_{HYD1} K_{H_2}^{1/2} P_{PAL} P_{H_2}^{1/2}]^2 \quad (S10) \end{aligned}$$

where  $k_{E1a}$ ,  $k_{E1b}$ , and  $k_{E1c}$  are the intrinsic rate constants for the rate controlling steps for paths  $E_{1a}$  (Cu-catalyzed H-elimination from the hemiacetalate intermediate),  $E_{1b}$  (H-addition to the hemiacetalate) and  $E_{1c}$  (coupling of surface propoxide and propanal);  $K_{C-O}$ ,  $K_{PAL}$ ,  $K_{Hadd}$ ,  $K_{HYD1}$  and  $K_{H_2}$  are the equilibrium constants for the for the coupling of the surface propoxide and propanal to form the C-O bond of the hemiacetalate, adsorption of propanal, hydrogen addition to the 1-propoxy-1-propoxide, hydrogenation of propanal to form the surface propoxide and the dissociative adsorption of hydrogen, respectively, and  $P_{AL}$  and  $P_{H_2}$  refer to the pressure of propanal and hydrogen, respectively.

The rate in path 3 (Fig. S4b) is characteristically different than those reported in paths 1 and 2 as the reaction proceeds by first activating the C-H bond of the adsorbed propanal to form a surface acyl ( $C_3H_5O^*$ ) intermediate that subsequently reacts with a vicinal propoxide to form the adsorbed propyl propionate. The results in Figure 8, indicate that the initial C-H activation step is quasi-equilibrated as the intrinsic barrier for the forward step involving the attack of the acyl on the vicinal bound propanal (85 kJ mol<sup>-1</sup>) is considerably higher than the barrier for the reverse reaction (60 kJ mol<sup>-1</sup>) involving the

hydrogenation of the bound acyl back to propanal. The rate for this route is therefore thought to be controlled by the coupling of the bound acyl and propanal surface intermediates and can be written as:

$$r_{E3} = k_{E3}K_{\text{acyl}}[\text{acyl}^*][\text{propanal}^*] \\ = k_{E3}K_{\text{acyl}}K_{\text{PAL}}^2K_{\text{HYD}}K_{\text{H2}}^{1/2}P_{\text{PAL}}^2P_{\text{H2}}^{1/2}/[1 + K_{\text{PAL}}P_{\text{PAL}} + K_{\text{PAL}}K_{\text{HYD}}K_{\text{H2}}^{1/2}P_{\text{PAL}}P_{\text{H2}}^{1/2}]^2 \quad (\text{S11})$$

where  $k_{E3}$ , refers to the intrinsic rate constant for the coupling of the surface propanal and acyl;  $K_{\text{acyl}}$ ,  $K_{\text{PAL}}$ ,  $K_{\text{HYD}}$ , and  $K_{\text{H2}}$  are the equilibrium constants for the C-H activation of propanal to form the surface acyl, the adsorption of propanal, the hydrogenation of propanal to form the surface propoxide over Cu, and the dissociative adsorption of hydrogen, respectively, and  $P_{\text{AL}}$  and  $P_{\text{H2}}$  refer to the pressure of propanal and hydrogen, respectively.

The results in Figure S4 along with the rate expression can be used to provide insights in the kinetics and the likelihood of the 3 paths. The results in section 3.2 concerning the propanal/propanol equilibrium suggest that the surfaces are covered with either propanal or propoxide intermediates. Experimental results indicate that the propanal is the most abundant surface intermediate. The detailed elementary step kinetics presented here are currently being used to develop microkinetic models that will aid in elucidating surface coverages and compositions and will be reported in a future communication.

For simplicity and in order to compare the different paths we make the assumption that the apparent barriers are measured with respect to adsorbed propanal and propoxide. As such, the elementary step activation and reaction energies for the different paths considered in Figures S4A and S4B are all taken with respect to adsorbed propoxide and propanal as the initial 0 energy reference state. The potential energy diagrams in Figure S4 along with the rate expressions derived in Equations S7-S11 indicate that the rate controlling steps for the  $E_{1a}$ ,  $E_{1b}$ ,  $E_{1c}$ ,  $E_2$  and  $E_3$  paths are H-addition to the hemiacetalate, the Cu-catalyzed C<sub>1</sub>-H activation, the nucleophilic attack of propoxide on adsorbed propanal, the simultaneous nucleophilic attack of propoxide on propanal together with H-elimination to Cu, and the coupling acyl and propanal, respectively. As such the apparent activation barriers for the  $E_{1a}$ ,  $E_{1b}$ ,  $E_{1c}$ ,  $E_2$  and  $E_3$  paths were calculated in Table 6 to be 76, 78, 60, 69 and 126 kJ mol<sup>-1</sup>. The apparent barriers for the  $E_{1a}$  (76 kJ mol<sup>-1</sup>),  $E_{1b}$  (78 kJ mol<sup>-1</sup>) and  $E_3$  (126 kJ mol<sup>-1</sup>) paths all appear to be rather high and unlikely paths. The rates for the  $E_{1c}$  and the  $E_2$  paths are both controlled by the initial attack on of the propoxide on the propanal and have barriers that are similar at 60 and 69 kJ mol<sup>-1</sup>, respectively and as such both are viable paths for esterification.

**Table S2.** The apparent rate constants and activation energies for the  $E_1, E_2$  and  $E_3$  esterification paths.

$k^{\text{app}}$	$Ea^{\text{App}}$	$Ea^{\text{intrinsic}}$ (kJ mol <sup>-1</sup> )	$\Delta E_{\text{rxn}}$ (kJ mol <sup>-1</sup> )	$Ea^{\text{App calc.}}$ (kJ mol <sup>-1</sup> )
$k_{1a} K_{\text{C-O}}$	$Ea_{1a} + \Delta E_{\text{rxn}}(\text{C-O})$	104	-28	76
$k_{1b} K_{\text{Hadd}}$	$Ea_{1a} + \Delta E_{\text{rxn}}(\text{Hadd})$	90	-12	78
$k_{1c}$	$Ea_{1c}$	60	-	60
$k_2$	$Ea_2$	69	-	69
$k_3 K_{\text{acyl}}$	$Ea_3 + \Delta E_{\text{rxn}}(\text{acyl})$			

The results reported here indicate that the ester is formed either by an  $E_{1c}$  path which involves a sequential mechanism where the rate-controlling C-O formation step, involving the coupling of a surface propoxide and propanal precedes a rapid hydride transfer from the alkoxide C-H bond to the vicinal bound propanal or by an  $E_2$  path which proceeds via the concerted coupling of a surface propoxide with coadsorbed propanal and direct hydrogen elimination to the surface. Both of these paths result in rate expressions and propanal and hydrogen dependencies that match those reported experimentally. [S4]

### S.6. Comparison of Condensation and Esterification Rates

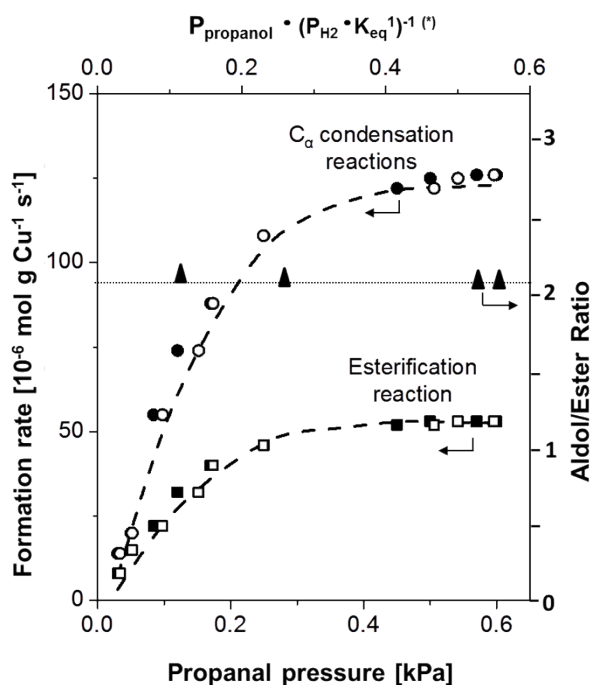


**Figure S5.** Aldol condensation (●) and esterification (□) formation rates from the reactions of propanal, hydrogen and propanol mixtures on 10% wt. Cu/SiO<sub>2</sub> catalysts with 5.5% dispersion are plotted (left axis) as a function of the propanal pressures (filled symbols) and  $P_{\text{propanol}} \cdot (P_{\text{H}_2} \cdot K_{\text{eq}})^{-1}$  (open symbols) where  $K_{\text{eq}}$  is the equilibrium constant for the interconversion of propanal-propanol at 503 K [60]. The symbols refer to the experimental data. The aldol to ester ratio (■) vs propanal pressure is reported on the right axis. Adapted from [S1]. Copyright 2011 American Chemical Society.

## References

- [S1] G. Kresse, J. Furthmuller, *Comput. Mater. Sci.* 1996, 6, 15.
- [S2] J. Perdew, *Phys.rev.B.*1992, 46, 6671.
- [S3] D. Vanderbilt, *Phys. Rev.B.* 1990, 41, 7892.
- [S4] M. E. Sad, M. Neurock, E. Iglesia, *J.Am.Chem.Soc.* 2011, 133, 20384.
- [S5] G. Mills, H. Jonsson, G.K. Schenter, *Surf. Sci.* 1995, 324, 305.
- [S6] H. Jónsson, G. Mills, K.W. Jacobsen, *World Scientific*, Singapore, 1998.
- [S7] G. Henkelman, B. P. Uberuaga, H. J. Jonsson, *J. Chem. Phys.* 2000, 113, 9901.
- [S8] G. Henkelman, H. Jonsson, *J. Chem. Phys.* 2000, 113, 9978
- [S9] G. Henkelman, H. Jonsson, *J. Chem. Phys.* 1999, 111, 7010.
- [S10] X. Qian, J. Li, L. Qi, C.Wang, T.Chan, Y.Yao, K. Ho, S. Yip, *Phys. Rew. B.* 2008, 78, 245112.
- [S11] B. Xu, X. Liu, J. Haubrich, R. J. Madix, C. M. Friend, *Angew. Chem. Int. Ed.* 2009, 48, 4206.
- [S12] B. Xu, J. Haubrich, T.A. Baker, E. Kaxiras, C. M. Friend, *J. Phys. Chem. C.* 2011, 115, 3703.
- [S13] X.Liu, B. Xu, J.Haubrich, R.J. Madix, C. M. Friend, *J. Am. Chem. Soc.* 2009, 131, 5757.